Analysis of the crustal structure of the Netherlands from receiver function inversion using the Neighbourhood algorithm

Ingrid Mulders, supervised by Hanneke Paulssen

April 20, 2013

Abstract

The crustal velocity structure beneath a station can be obtained from seismograms by constructing receiver fcuntions. Receiver functions eliminate the source time function and the instrument response so that only the near receiver Earth reponse is left. The inversion of these receiver functions is highly non-linear and non-unique. The Neighbourhood algorithm can be used for this inversion, since it is based on random choice of model samples, though uses the misfits of the previous models in the search for the optimum model. In this study, the method of inverting receiver functions by the Neighbourhood algorithm is tested for the determination of the crustal velocity structure of the Netherlands. Data from stations NE05 (Utrecht) and NE014 (Beuningen) from the temporary network NARS-Netherlands is used. For station NE05 the most data is available, though the thick sediments decrease the signal-to-noise ratio. Station NE014 is chosen for its thin sediment layer despite the lack of data compared to NE05.

The found velocity structures depend clearly on the choice of the model parameters. These are the deconvolution parameters, the Neighbourhood algorithm parameters and the number of layers of the parameterisation model.

The subsurface of the Netherlands is heterogeneous and/or anisotropic as becomes clear from the receiver functions. They differ between stations and between events. In addition, the transverse components show a relatively high seismic energy level. The sediment layer beneath the Netherlands is visible in the receiver functions from the time shift of the first peak by 1-2 s. For station NE014, the sediment layer is well resolved, while the deeper structure is not. Beneath station NE05 both the sediments and a mid-crustal velocity contrast are found, though the Moho is not determined. Two factors make the method not ideal for the Netherlands. First, the dominance of the complex sediments in the receiver functions prevents good determination of the deeper structure. Second, the lack of data, especially for station NE014, makes it hard to construct proper stacks and the small range in both slowness and azimuth obstructs the solution of trade-offs and heterogeneity.

Contents

1 Introduction

Numerous studies have been done on the shallow subsurface of the Netherlands [25, 27, 5]. These studies are based on borehole data and seismic reflection lines and show a detailed structure of the approximate 3 km thick sedimentary basin present below the Netherlands. On the other hand, how the structure looks beneath these sedimentary layers is hardly known. Such information will give more insight in the geological processes acting beneath the Netherlands.

The thickness and structure of the sediment layer is determined in great detail for both the onshore and offshore part of the Netherlands from borehole data and seismic reflection lines [5, 25]. The sediments have a thickness of 1 to 3 km, with local basins up to 5 km. In general, the sediment layer is thinner in the eastern part of the Netherlands compared to the western, offshore part. Several faults and fault zones have been found in the shallow subsurface of the Netherlands. These faults are all shallow and located far enough from the analydes stations, NE05 and NE014 in figure 1, so that they do not have influence on the recorded seismograms. Dalfsen et al. [27] determined the P-wave velocity structure of the sediments using borehole data. The average P-wave velocities of the sediments was found to be 3.0-3.5 km/s with a sharp decrease to 2.0 km/s at the transition from the shallow North Sea groups to the Chalk group.

Besides studies based on borehole data and seismic lines, receiver functions are used to determine the structure beneath the Netherlands (only the onshore part) [28, 18]. Receiver functions (RFs) are constructed by isolating the near receiver Earth response from the seismograms. In the study of van Dedem [28] the sediment layer was determined in the central-eastern part of the Netherlands and has a variable thickness of 1.3 to 3.5 km. Further, a mid-crustal discontinuity was found at a few stations at a depth of ~10 km and the depth of the Moho was determined to be 32-35 km. The Moho was not determined for the central and western part of the Netherlands. The study of Paulssen et al. [18] used a method similar to the RF method to determine the crustal structure beneath station NE05 (Utrecht) located in the middle of the Netherlands. Three major discontinuities were found: a transition from sediment to crust at a depth of 1.0-1.5 km, a mid-crustal transition at 11 km and the Moho discontuity at a depth of 27 km. The corresponding P- and S-wave velocities were determined as well. In Germany the depth of the Moho is determined by migrating the RFs, which are time series, into spatial images [10]. A crustal thickness varying between 30 and 38 km was found.

Furthermore, deep seismic reflections have been performed in the Netherlands to determine the crustal structure [4], though the quality of the reflections were not good enough to properly determine the depth of the Moho. A more recent study in Belgium based on phases reflected at the Moho from local earthquakes showed that the Moho is located at a depth of 31 km in Belgium [23].

The aim of this study is to find a good method to determine the crustal velocity structure of the Netherlands. Other studies [33, 32, 29] have determined the crustal structure succesfully from receiver functions (RF), the isolation of the near receiver Earth response from a seismogram. The travel time differences between phases reflecting and converting at the Moho can be used to obtain the thickness of the crust [33, 31, 29]. More popular is the inversion of RFs. Different inversion techniques are used: the Monte Carlo algorithm [28, 26], least squares inversion [30], simulated annealing [15] and the Neighbourhood algorithm (NA) [8, 32]. In this study the inversion of receiver functions using the Neighbourhood algorithm is tested as a method to determine the crustal velocity structure of the Netherlands. The Neighbourhood algorithm is chosen, fot it is based on random choice, though uses the misfits of previous models in the search for the optimum model. This study will first optimize and test this method by performing synthetic tests. Next, the method will be applied to two stations of the temporary seismic network NARS-Netherlands. This network has been active from 2008 up to 2012 and consists of 19 temporary stations and one permanent station, station NE05 (see figure 1 and check *http://www.geo.uu.nl/∼seismain/*). Two stations have been chosen, NE05 (Utrecht) and NE014 (Beuningen) for they have a larger amount of data and a high signal-to-noise ratio, respectively.

Figure 1: The seismic stations of the temporary network NARS-Netherlands.

2 Theory

In this section the theory of the receiver function inversion method is explained. First, the construction of receiver functions is handled, followed by an explanation of the exact working of the Neighbourhood algorithm.

2.1 Receiver functions

Seismograms of different events are used to construct a velocity model of the subsurface of the Netherlands. These events will have different source time functions so can not be compared directly to each other. In this study the receiver function technique, developed by Langston [14], is used to remove the source time function from the seismogram. Here, the method will be explained.

A seismogram can be written as the convolution of three parts: the source time function, the Earth response and the instrument response.

$$D_r(t) = S(t) * E_r(t) * I(t) \tag{1}$$

where $D_r(t)$ and $E_r(t)$ stand for the radial components of the ground displacement and the Earth impulse reponse, respectively, $S(t)$ for the source time function and $I(t)$ for the instrument impulse response. Similar formulas can be obtained for the vertical, $D_v(t)$, and transverse, $D_t(t)$, components.

For the analysis of the Earth's structure, both the source time function and the instrument response need to be filtered out, which can be done with deconvolution. The displacement response is divided by the source time function and the instrument response in the frequency domain.

$$E_r(\omega) = \frac{D_r(\omega)}{S(\omega)I(\omega)} \tag{2}$$

When only teleseismic data are used, so that the ray has a nearly vertical incidence, the vertical component of ground motion can be approximated as the source time function convolved with the instrument response. Theoretical calculations of Langston [13] show that the vertical ground motion is almost the same for a horizontal crustal structure as for a structure with a 10° dipping Moho, because the amplitude of converted phases and crustal reverberations is very small on this component. This approximation is valid for very large velocity contrasts (up to ∼2 km/s) as well [17].

$$D_v\left(t\right) \simeq S\left(t\right) * I\left(t\right) \tag{3}$$

Now, the Earth response given above becomes:

$$E_r\left(\omega\right) \simeq \frac{D_r\left(\omega\right)}{D_v\left(\omega\right)} \tag{4}$$

$$E_t\left(\omega\right) \simeq \frac{D_t\left(\omega\right)}{D_v\left(\omega\right)} \tag{5}$$

Then, the radial and transverse components of the receiver functions are the time series corresponding to $E_r(\omega)$ and $E_t(\omega)$.

This deconvolution is numerically unstable, since the product of the source time function and the instrument response in the frequency domain can be very small resulting in a division through nearly zero. Therefore an estimation of the deconvolution is used. The radial component of the RF in the frequency domain then becomes:

$$E_r(\omega) = \frac{D_r(\omega)D_v^*(\omega)}{\Phi(ss)} \cdot G(\omega) \tag{6}$$

with

$$\Phi(ss) = \max \left\{D_v(\omega)D_v^*(\omega),\ c \max\left[D_v(\omega)D_v^*(\omega)\right]\right\} \tag{7}$$

and

$$G(\omega) = e^{-\omega^2/4a^2} \tag{8}$$

where $D_v^*(\omega)$ is the complex conjugate of $D_v(\omega)$. The function $\Phi(ss)$ denotes the autocorrelation of the vertical displacement in the frequency domain, where c, the water level, is introduced to avoid division through very small numbers. This parameter fills any spectral throughs. Usually c is chosen as small as possible for which the deconvolution is still stable.

The approximated deconvolution is multiplied by a Gaussian filter to eliminate the highest frequencies which resulted from the deconvolution. The width of the Gaussian, α, determines the amount of detail of the receiver function. A Gaussian with a lower α filters out higher frequencies and is thus less detailed than one with a higher value for α. Other filters can be used as well (e.g. the extended-time multitaper method [22]), but these make the RF less smooth.

Since the radial component is divided by the vertical component in the frequency domain, receiver functions show only P-to-S conversions, except for the direct P-arrival [1, 33]. Large velocity contrasts such as at the Moho result in high amplitude P-to-S conversions and will thus show up clearly on the RF.

2.2 Neighbourhood algorithm

The inversion of waveforms is found to be highly non-linear and often shows ambiguous results [2, 19]. Therefore a different inversion technique than linearized approximation is preferred. A random search method, as the Monte Carlo technique, will give the best model in the end, but costs a lot of computation time. The Neighbourhood algorithm (NA) [19, 20] is a similar method as genetic algorithms [9] and simulated annealing [6] and is a good alternative for highly non-linear inversion problems such as the inversion of RFs.

The NA starts with a selection of n_s randomly chosen model samples. The model space is then divided in Voronoi cells (i.e. nearest neighbour regions around the model samples) with the chosen model samples as midpoints. For these models synthetic RFs are constructed using the Thomson-Haskell forward modelling approach

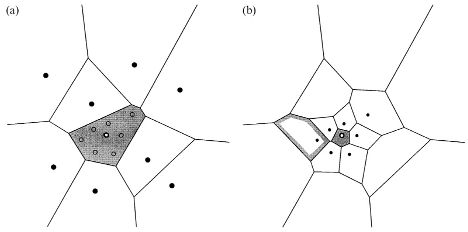

Figure 2: An example of how the Voronoi cells change shape and can grow out of their previous Voronoi cell. (a) Nine sample points and their Voronoi cells. In the shaded cell, seven points are added. (b) The new generation Voronoi cells have decreased in size and have crossed the boundaries of the original Voronoi cell. [19]

technique [24, 11] and the misfit between the synthetic and observed RFs is calculated. In the next iteration synthetic RFs are construced for a new set of n_s models. This selection of models is dependent on the calculated misfit surface. New models will be selected using the n_r models of the previous set with the lowest misfit. Then a random walk through the corresponding Voronoi cells, with the previous model as starting point, is used to select the next model samples (i.e. n_s/n_r models per Voronoi cell). In this way more models in a region with a low misfit will be selected than in one with a high misfit and the inversion will converge towards the optimum model.

The advantage of the NA above genetic algorithms and simulating annealing is that only three model parameters are involved: the amount of iterations, n_{iter}, the amount of model samples in each iteration, n_s, and the amount of resampled models, n_r. Because only these three parameters need to be set, the NA can be optimized well. Further, the information of previous models is used in a rather easy way compared to simulated annealing and genetic algorithms, which saves computation time. Finally, no scaling of the misfit functions is used in the NA, since only the ranking of the misfit function is imoprtant. In both simulated annealing and genetic algorithms the absolute value of the misfit function is used and therefore scaling of the misfit function is required.

In the case of inversion of RFs the model space consists of three model parameters per layer: the S-velocity, the $v_p - v_s$ ratio and the thickness of the layer. The halfspace at the bottom of the pile of layers, representing the mantle, has only two model parameters, v_s and v_p/v_s. In the case of a four-layer model (half-space included) the model space has eleven dimensions. Note that this approach differs slightly from the RF application of Sambridge [19]. This study uses four model parameters per layer, namely the S-velocity at both the top and the bottom of the layer assuming a linear gradient throughout the layer. Since the vertical velocity variations inside each layer will have only minor effects on the shape of the RF compared to the velocity changes across layer boundaries, this vertical velocity variation is left out here and the amount of model parameters is decreased.

The forward model used is the Thomson-Haskell propagation matrix method. The density necessary for the forward model is obtained from the P-velocity as described by Brocher [3]. The forward model has a serious limitation, since it can only handle isotropic, homogeneous, flat layers.

Besides inversion of a single RF, the RF inversion is adapted such that a joint inversion of various RFs is possible. This changes the misfit calculation, since the misfit needs to be divided by the amount of RFs. Furthermore, stacks of RFs are used and therefore the standard deviation of these stacks, σ_{stack}, is implemented in the χ^2-misfit calculation as well:

$$\chi^2 = \frac{1}{n_{wave}} \frac{1}{n_{data}} \sum_{i=1}^{n_{wave}} \sum_{j=1}^{n_{data}} \left(\frac{d_{obs_{i,j}} - d_{pred_{i,j}}}{\sigma_{stack_{i,j}}} \right)^2 \tag{9}$$

where n_{wave} and n_{data} are the amount of RFs and datapoints per RF, respectively, and $d_{obs_{i,j}}$ and $d_{pred_{i,j}}$ are the values of the observed and predicted RFs, respectively. The time window, Δt, over which the misfit is calculated can be adapted in the NA. A misfit of $\chi^2 \leq 1$ means that the data can be explained by the velocity model within their error bar. Therefore not only the model with the lowest misfit, the best model, is important, but all models with a misfit of $\chi^2 \leq 1$. This ensemble of models shows how well defined the velocity structure is and whether the solution is unique or not. To get a good insight in the resolution of all the model parameters, probability density functions can be constructed [20]. These functions show per model parameter the probability that a certain value is the correct value. These functions will not be computed here, but can certainly be useful in future studies.

Since the inversion of RFs is highly non-linear, the main issue of the inversion is entrapment in local minima. At first glance it seems that the NA would struggle moving out of local minima, although if n_r is chosen large enough, the NA is explorative enough to find the absolute minimum. Further, the Voronoi cells change every iteration, since new model spots enter the model space and the amount and shape of the Voronoi cells change. Figure 2 shows that a newly constructed Voronoi cell can grow out of the previous one. In this way the NA can move away from local minima.

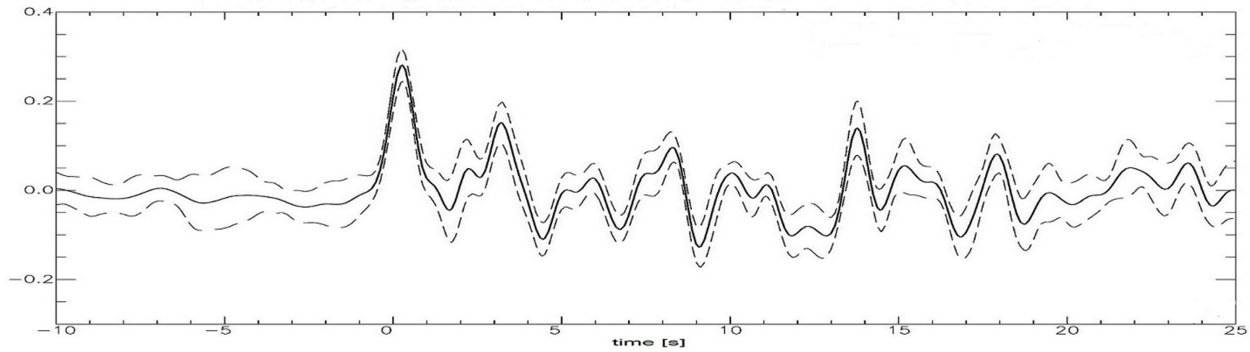

Figure 3: Stacked receiver function (solid line) with twice its standard deviation (dashed lines) for station NE014. $\alpha = 2$, $c = 0.001$, baz = 0° - 90°and $s = 0.045 - 0.050$ s/km.

Station	Location	Latitude	Longitude
NE05	Utrecht	52.08746 N	5.17098 E
NE014	Beuningen	52.34197 N	7.05671 E

Table 1: Stations of the NARS-Netherlands network used in this study

3 Data

Data assembled by the NARS-Netherlands network is used. Two of the stations are selected. First station NE05, which is located in the middle of the Netherlands. This station has a reasonable noise level and has been active since 2001. The second station is NE014 at the eastern border of the Netherlands. The seismograms are of high quality having a low noise level. This station has been operating over a shorter time period, from November 13 2009 to October 4 2012. The exact locations of the stations can be found in table 1.

For the construction of RFs only teleseismic events can be used. Therefore events with an epicentral distance of $\Delta = 40^{\circ} - 90^{\circ}$ (i.e. an epicentral

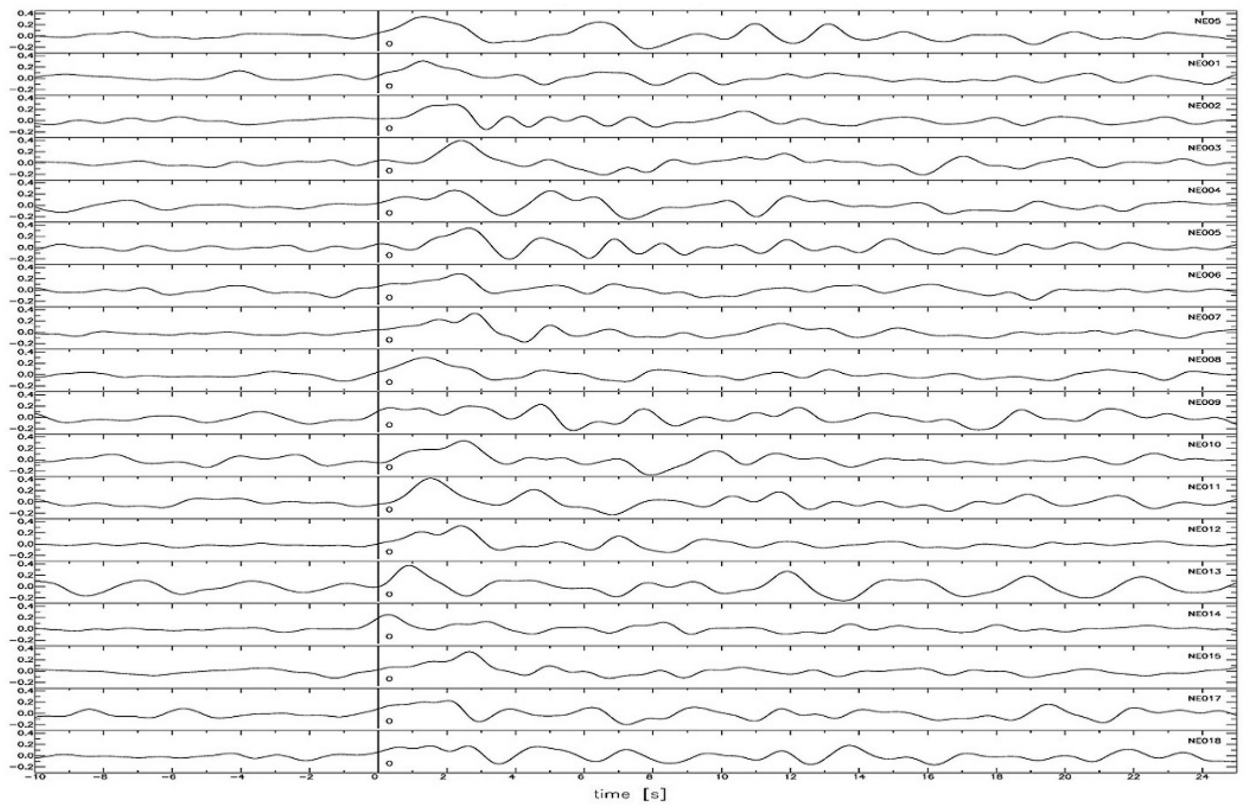

Figure 4: Receiver functions for the event at 11 March 2011 at Tohoku, Japan for all stations of the NARS-Netherlands network.

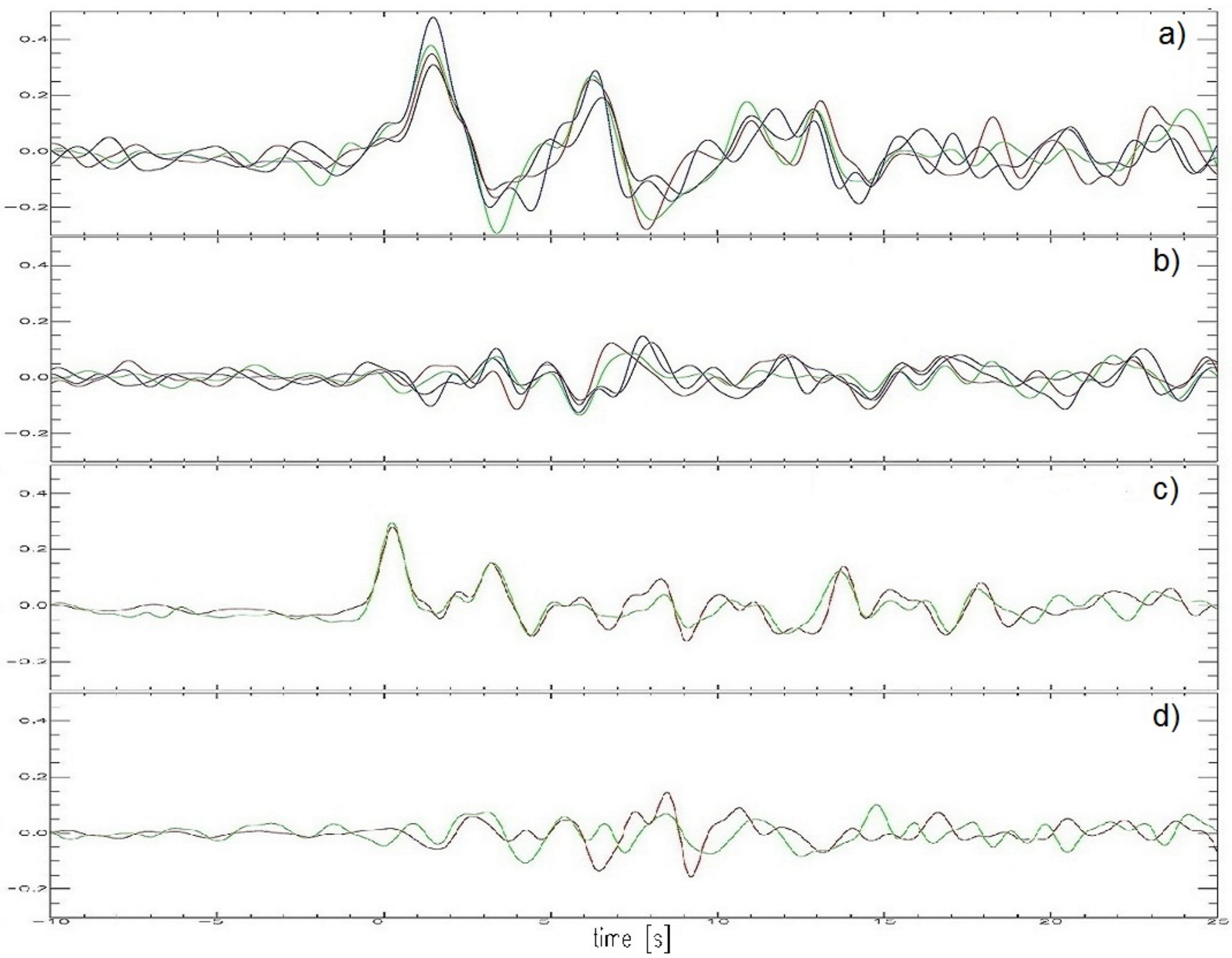

Figure 5: Stacked receiver functions for different slownesses (black - s = 0.040 − 0.045 s/km, red - s = 0.045 − 0.050 s/km, green - s = 0.045 − 0.050 s/km and blue - s = 0.065 − 0.070 s/km) for α = 2, c = 0.001 and baz = 0° - 90°. (a) Radial components NE05. (b) Transverse components NE05. (c) Radial components NE014. (d) Transverse components NE05.

distance > 4400 km) are selected. Further, all events have a magnitude of 6.0 or more, so that the seismograms should have a reasonable singal-to-noise ratio. During picking of the P-arrivals and after construction of the RFs only the best events are selected based on the amount of noise before the first arrival and on the similarity between the RFs. For station NE014 fifteen events were selected and 65 events for station NE05 (see appendices A and B).

The events are divided in clusters of slowness, s. Seven clusters are made starting at $s = 0.040$ s/km (i.e. $\Delta \simeq 90$ °) with intervals of 0.005 s/km. Next, the events are grouped in quadrants of back azimuth as well, since the RFs differ with back azimuth. Stacks are made per slowness-back azimuth cluster to increase the signal-to-noise ratio of the RFs. Another advantage of stacking is that the variance of the data can be implemented in the inversion. An example of a stack is shown in figure 3 for staion NE014 along with twice its standard deviation. The area in between the dashed lines represents the 95% confidence interval. The synthetic RFs of the neighbourhood algorithm should thus fall in this area. To be able to construct a good stack, enough RFs need to be available. This is not the case for the back azimuth groups SE, SW and NW and for some slowness clusters in the NE group. In figure 5 the stacks with high enough quality are given for both stations. Since there is less data available for station NE014, proper stacks for only two slowness clusters could be made against four for station NE05. The amount of RFs per stack, which is a representation of the quality of the stack, is as well less for station NE014: 4 to 11 RFs are used per stack for station NE014 and 9 to 27 RFs for station NE05.

Two differences between station NE05 and NE014 become clear from figure 5. First, the stacked RFs of station NE05 all have higher amplitudes. Secondly, the dominant period of these stacks is larger than for the stacks of NE014. Further, the stacks show indications for a heterogeneous or anisotropic subsurface, since there is a high amplitude level on the transverse component. In addition, the RFs vary with back azimuth for a single station and there is large variation between several stations for a single event as well as shown in figure 4 [8, 16]. Unfortunately, there is not enough azimuthal spreading in the data to determine the exact cause of this variation, for the most events come from the NE [16, 15, 13]. Finally, the first peak is shifted in time by 1-2 s for both stations, which is an effect of the thick sediment layer [30, 29] present in the Netherlands.

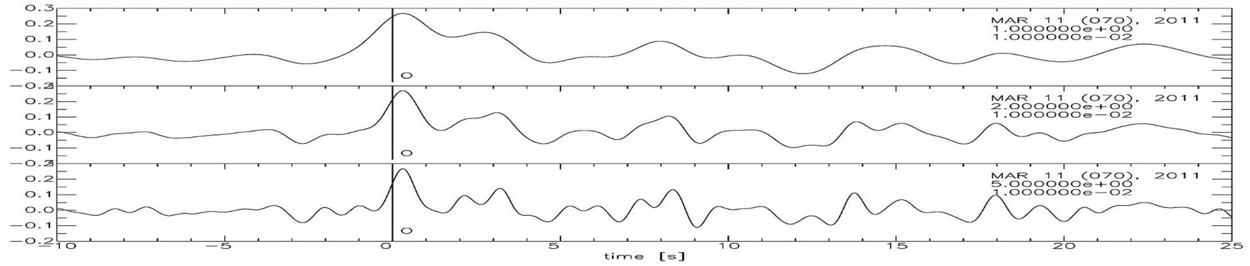

Figure 6: The radial components of the receiver functions for station NE014 for increasing α for the event at 11 March 2011 in Tohoku, Japan. alpha increases from top to bottom from 1 to 2 to 5 and $c = 0.01$.

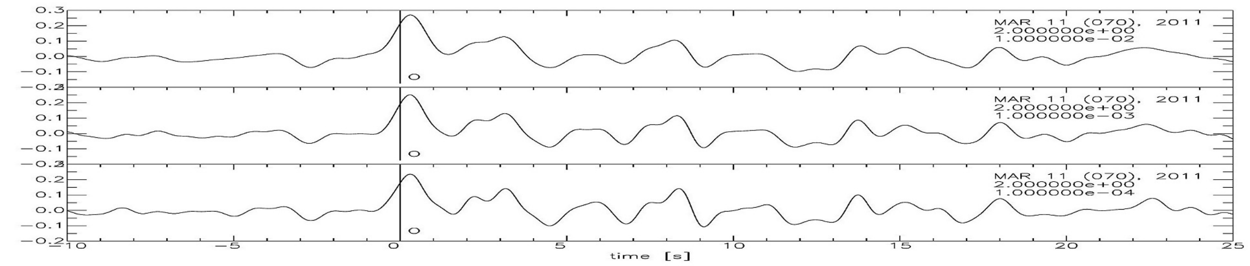

Figure 7: The radial components of the receiver functions for station NE014 for decreasing c for the event at 11 March 2011 in Tohoku, Japan. c decreases from top to bottom from 0.01 to 0.001 to 0.0001 and $\alpha = 2$.

4 Methods

4.1 Setting the Gaussian parameters

Now, the Gaussian parameters, α and c, are determined. They are chosen such that the receiver functions of a single station are very similar but maintain a sufficient level of detail. The RFs of ten events (see table 7 in appendix C) recorded at both stations NE05 and NE014 are compared for each station.

The value for α is varied between 1 and 5, which corresponds to frequencies of 0.05 and 2.4 Hz, and the water level value between 0.01 and 0.0001. In figures 6 and 7 the RFs for different values of α and c are shown. From these figures it is clear that the width of the Gaussian has more influence on the shape and amount of detail of the receiver functions than the height of the water level. We found the best combination of good similarity between the receiver functions and still sufficient detail for $\alpha = 2$ and $c = 0.001$ (figure 8).

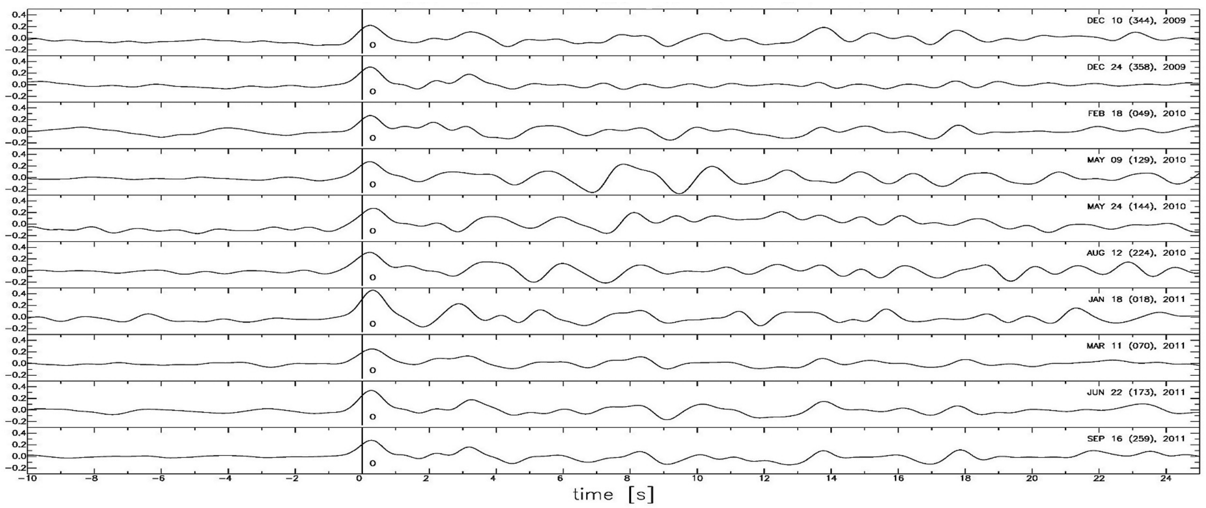

Figure 8: Radial components of the receiver functions for the ten events given in tabel 7 in appendix C for station NE014, $\alpha = 2$ and $c = 0.001$.

4.2 Synthetic tests

In this section both the NA is tested as a inversion technique for the RFs and the NA is optimized by setting the values for n_{iter}, n_s and n_r. This is done by running synthetic tests in which a known velocity structure is used to construct RFs. The NA is used with different values for n_{iter}, n_s and n_r for these RFs. Comparison of the modelled and start velocity structures will show whether the NA can be used for the inversion of RFs and will provide information on the best combination of NA parameters.

The effect of n_{iter} on the performance of the NA is quite clear. For a higher value of n_{iter} the algorithm will have more time to converge towards the minimum misfit. The value of n_r influences the explorativity of the NA. A larger n_r will lead to a more explorative search, while a small n_r leads to a more local search to find a better optimal model with the risk of getting trapped in a local minimum. As a consequence of a higher n_s more locations in the model space will be searched thoroughly, because the number of new model samples per Voronoi cell increases. This can avoid entrapment in local minima as well.

Different slownesses can be used for the construction of the RFs. A ray with a low slowness falls in almost vertically, so that the first P-arrival has a relatively high amplitude, while the P-to-S conversions will be less pronounced on the seismograms. At first a relatively high slowness of 0.070 s/km is chosen. Runs with the same NA and Gaussian parameters but with RFs constructed with different slownesses showed that the misfit between the original and predicted RFs increases linearly with increasing slowness. For a ray with a lower slowness the P-to-S conversions will have smaller amplitudes on the RFs. Therefore, a small deviation from the real Earth structure will only have a minor effect on the difference between the original and predicted RF compared to a ray with a higher slowness.

For the synthetic tests three different four-layer models are used consisting of sediments, upper crust, lower crust and mantle. The exact velocities and thicknesses of the layers are shown in table 2. The three columns at the right side give the model parameters as predicted by the NA.

Figure 9 shows all models analysed by the NA, where the colours represent the misfit between the original and modelled RFs. On the axes the model parameters for the four different layers are given. The red cross shows the true model and the blue one the optimum model found by the NA. These are very similar here. Further, the figure shows whether the whole model space is searched. If this is not the case, n_r is increased. The stability of the inversion is analysed by taking different velocity structures and varying starting sets of randomly chosen models. Good fits between the modelled and true velocity models are obtained for a wide range of values of n_{iter}, n_s and n_r indicating that the NA is a good technique to invert RFs. However, a significant positive trade-off between the thickness, h, and the

Velocity model 1						
	Input velocity model			Predicted velocity model		
Layer	V_s [km/s]	V_p/V_s	Thickness [km]	V_s [km/s]	V_p/V_s	Thickness [km]
1	1.60	2.50	3.0	1.44	2.54	2.72
2	3.00	2.00	14.0	2.82	2.01	13.16
3	3.60	1.80	13.0	3.40	1.82	12.22
4	4.40	1.70	-	4.22	1.64	-
Velocity model 2						
	Input velocity model			Predicted velocity model		
Layer	V_s [km/s]	V_p/V_s	Thickness [km]	V_s [km/s]	V_p/V_s	Thickness [km]
1	1.40	2.40	1.0	1.38	2.54	1.01
2	3.20	2.10	14.5	3.19	2.11	14.26
3	3.50	1.70	15.0	3.50	1.71	15.26
4	4.70	1.65	-	4.69	1.64	-
Velocity model 3						
	Input velocity model			Predicted velocity model		
Layer	V_s [km/s]	V_p/V_s	Thickness [km]	V_s [km/s]	V_p/V_s	Thickness [km]
1	1.30	2.55	4.0	1.20	2.59	3.72
2	2.90	1.90	12.0	2.78	1.91	11.58
3	3.60	1.70	16.0	3.45	1.70	15.20
4	4.50	1.60	-	4.33	1.57	-

Table 2: Velocity models used for and predicted by the synthetic tests. $\alpha = 2.0$, $c = 0.001$, $s = 0.07$ *s/km,* $n_{iter} = 2000$, $n_s = 20$ *and* $n_r = 15$.

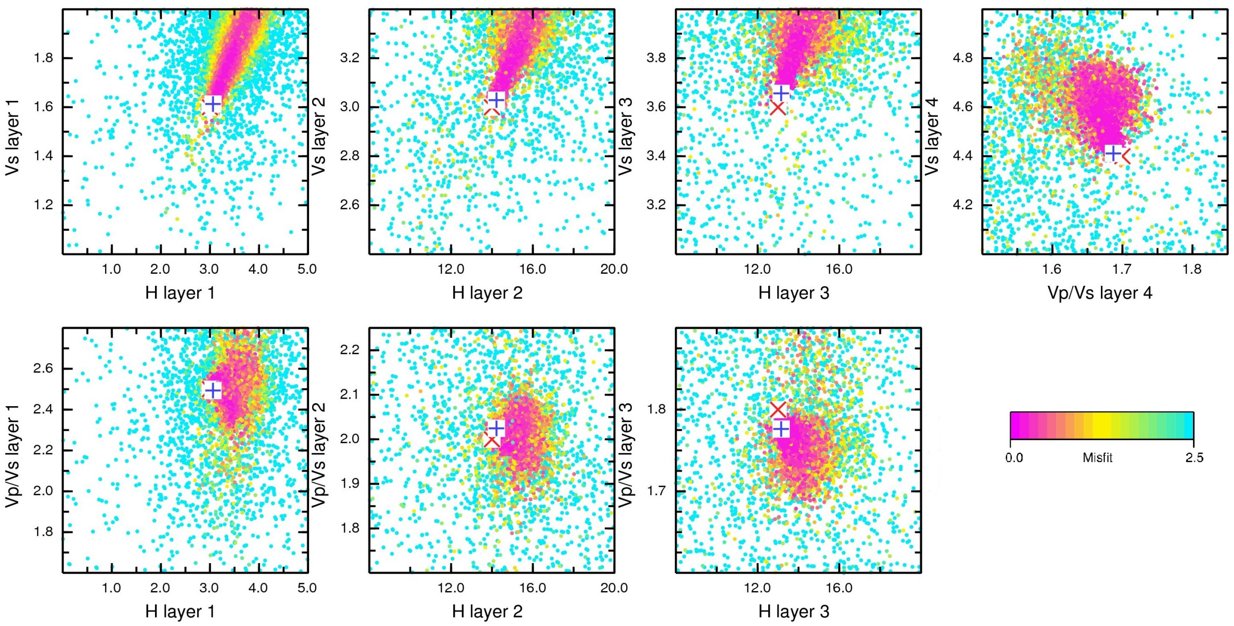

Figure 9: Plots of all NA model samples with their misfits for the first velocity model. On the axes the model parameters for the four different layers are given. The red cross represents the true model and the blue corss the optimum model. $n_{iter} = 2000$, $n_s = 20$ *and* $n_r = 15$.

shear wave velocity, v_s, exists. The trade-off can be minimized by taking RFs over a range of slownesses, if available [33, 17]. The velocity ratio v_p/v_s shows a relatively large range of good models and is thus less well determined.

The RFs constructed from the starting velocity models and the corresponding RFs constructed by the NA are given in figure 10 for the three different input models. The fits between the original and the modelled RFs are nearly perfect. Interesting to see are the variations between the three input models. Very good fits between the RFs are found for $n_s = 20$, $n_r = 15$ and $n_{iter} = 2000$. A smaller number of iterations gives misifits of the same order, but is less stable for different starting sets of models. From the good fits both between the original and modelled RFs and between the true and predicted models it is clear that the inversion of RF by the NA is a good method to obtain the crustal velocity structure beneath a seismic station.

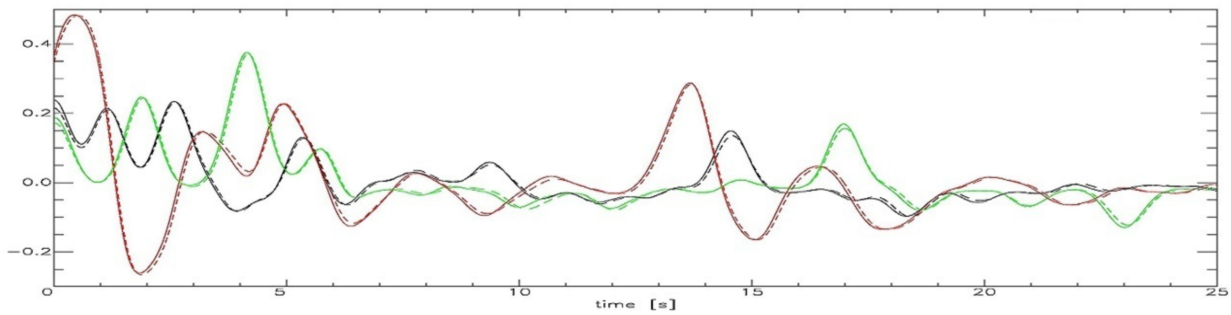

Figure 10: Receiver functions constructed from the three input velocity models (solid lines: model 1 - black, model 2 - red and model 3 - green) and the optimum NA velocity models (corresponding dashed lines) with $\alpha = 2.0$, $c = 0.001$ *and* $s = 0.07$ *s/km.*

5 Results

Several sets of runs have been done for both stations in the search for the crustal velocity model of the Netherlands and to see what the effects of the different parameters are on the search. The parameterisation model is adapted several times based on the outcome of the previous models. If the search converged to one of the sides of the model space, then the range of the model space had to be increased. The effect of the amount of layers is tested by taking four-, five- and six-layer parameterisation models. The values found for the Gaussian and NA parameters are used and a time window, Δt, of 25 s. First, the results of station NE014 are presented for three different parameterisation models.

5.1 Station NE014

For station NE014 only two slowness clusters are used: $s = 0.045 - 0.050$ s/km ($\Delta = 85^{\circ}-78^{\circ}$) and $s = 0.050 - 0.055$ s/km ($\Delta = 78^{\circ}-70^{\circ}$), both with a NE back azimuth. The other slowness clusters did not have enough events for the construction of a good stack. The quality of the stacks is reasonable, though only four to eleven RFs are used per stack (see appendix B). Runs are performed for each stack separately as well as simultaneously. Overall lower misfits are obtained for the single inversions. Still, we represent here only the results of the joint inversions, for these are based on the largest amount of data and thus provide the most information on the structure of the crust.

5.1.1 Influence of parameterisation models

Three different parameterisation models are tested for station NE014. The specifications of the models are given in table 3. The velocity models found by the NA are given in figure 11. The grey lines represent all the model samples analysed by the NA, the coloured lines are all the model samples which resulted in a misfit smaller than one and the red line is the best model. If there is no model with a misfit smaller than one, then the best 1000 models are plotted. In all three velocity plots a shallow thin low-velocity layer is found, the sediment layer. It has a thickness of $\sim$ 1 km and a S-wave velocity of $\sim$ 1.2 km/s. The deeper velocity structure differs for the three parameterisation models, so the runs give inconsistent results. Furthermore, the misfits between the observed and synthetic receiver functions are all larger than one, so none of the models can explain the data. The range of models with a relatively low misfit increases for an increasing number of layers.

In figure 12 the observed and predicted RFs are given for the three different parameterisation models. The predicted RF for the four-layer parameterisation model differs a lot from the observed RF, especially the first peaks have different amplitudes and are shifted in time. The predicted RFs for the five- and six-layer models show better similarity, but most peaks still have slightly different amplitude, timing or frequency. The fit to the observed RF decreases with increasing time.

Inspection of the plots of all the model samples in the model space shows that it is searched well for all three parameterisation models, although some

Parameterisation model 1			
Layer	V_s [km/s]	V_p/V_s	Thickness [km]
1	0.6 - 2.8	1.70 - 3.20	0 - 4
2	2.2 - 3.8	1.00 - 2.60	7 - 20
3	2.2 - 4.0	1.00 - 2.40	3 - 20
4	2.5 - 5.0	1.00 - 2.00	5 - 50
Parameterisation model 2			
Layer	V_s [km/s]	V_p/V_s	Thickness [km]
1	0.6 - 2.8	1.70 - 3.20	0 - 4
2	2.2 - 3.80	1.00 - 2.60	3 - 20
3	2.2 - 4.0	1.00 - 2.40	3 - 20
4	2.2 - 4.0	1.00 - 2.40	3 - 20
5	2.5 - 5.0	1.00 - 2.00	5 - 50
Parameterisation model 3			
Layer	V_s [km/s]	V_p/V_s	Thickness [km]
1	0.6 - 2.8	1.70 - 3.20	0 - 4
2	2.2 - 3.8	1.00 - 2.60	3 - 20
3	2.2 - 4.0	1.00 - 2.40	3 - 20
4	2.2 - 4.0	1.00 - 2.40	3 - 20
5	2.2 - 5.0	1.00 - 2.40	3 - 20
6	2.5 - 5.0	1.00 - 2.00	5 - 50

Table 3: Parameterisation models of the NA.

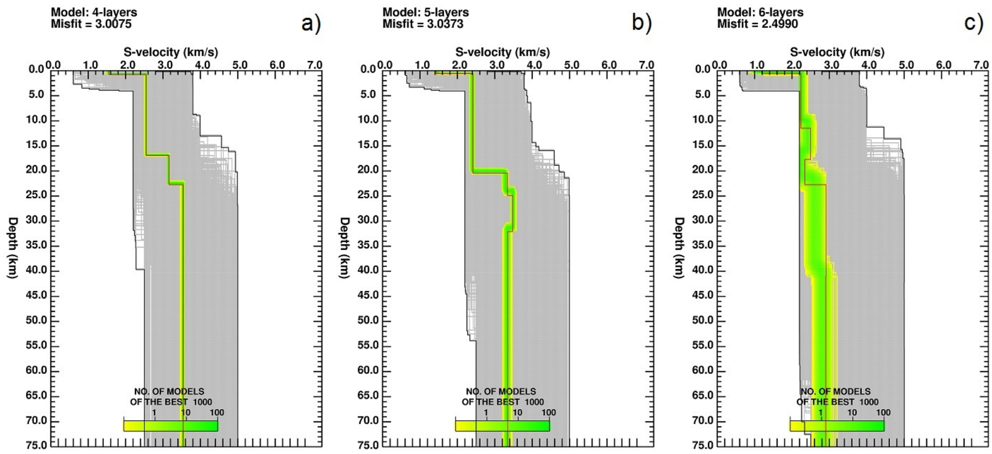

Figure 11: Velocity models for three different parameterisation models for station NE014. $\alpha = 2$, $c = 0.001$, $\Delta t = 25$ s, $n_{iter} = 2000$, $n_r = 20$ and $n_s = 15$. (a) Four-layer model. (b) Five-layer model. (c) Six-layer model.

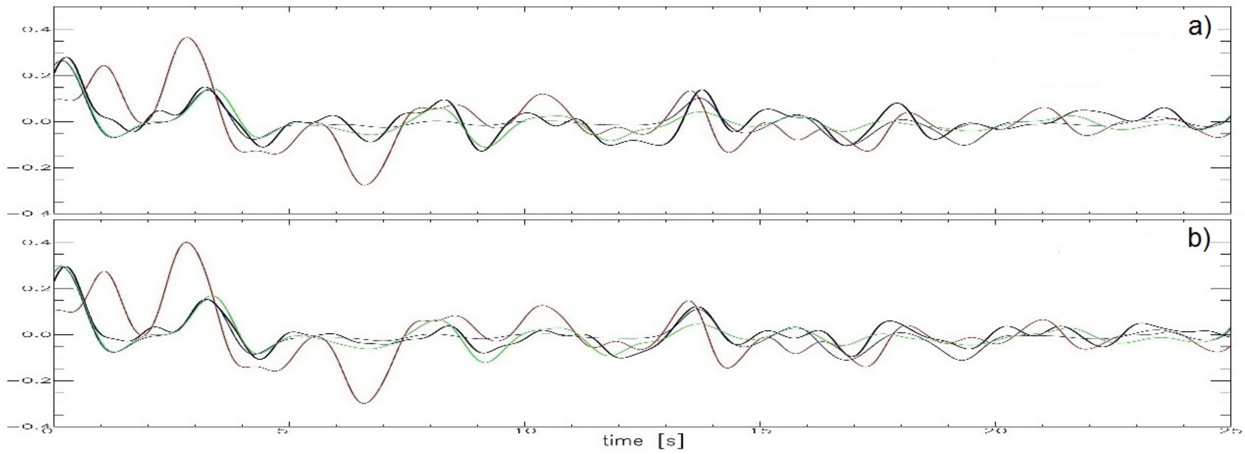

Figure 12: Observed (black) and predicted (red - model 1, blue - model 2, green - model 3) receiver functions for station NE014 for $\alpha = 2$, $c = 0.001$, $n_{iter} = 2000$, $n_r = 20$ and $n_s = 15$. (a) $s = 0.045 - 0.05$ s/km. (b) $s = 0.05 - 0.055$ s/km.

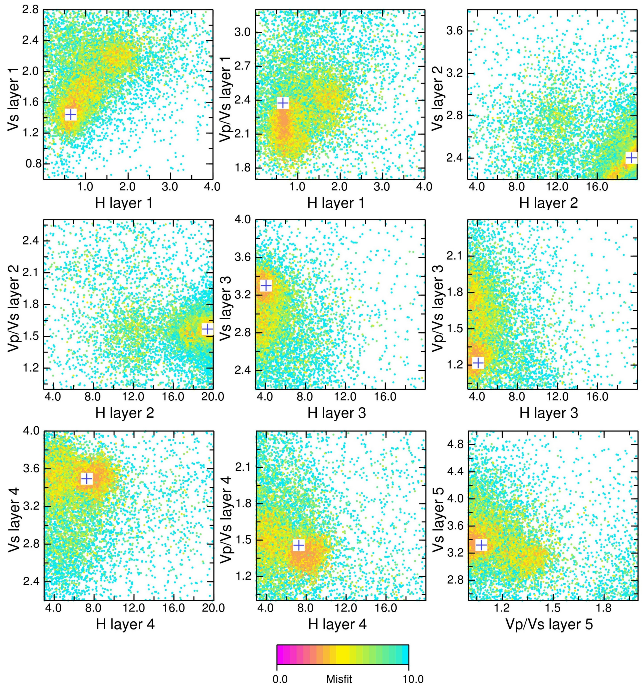

Figure 13: Plot of all model samples analysed by the NA with their misfits. On the axes the model parameters are given. Run for staion NE014 for parameterisation model 2, $\alpha = 2$, $c = 0.001$, $\Delta t = 25$ s, $n_{iter} = 2000$, $n_s = 20$ and $n_r = 15$.

spots could be sampled a bit more. In figure 13 an example is given for the five-layer parameterisation model. A small trade-off is visible between h and v_s, especially in the first two layers. Presence of large ranges of model samples with relatively low misfit values and occurence of secondary minima for the five- and six-layer model in the lowest layers indicate ambiguity. Sometimes the model search is stuck at one of the sides of the model space. This can partly be solved by increasing the ranges of the model space, but sometimes it can be hard for the NA to move away from the sides.

5.1.2 Influence of NA parameters

Since all the misfits were above one, the previous runs weren't able to explain the data. Further, the deeper structure is not resolved. To increase the qualtiy of the data, the NA search is made more explorative by setting new NA parameters, NA2: $n_{iter} = 1000$, $n_s = 150$ and $n_r = 50$. The Gaussian parameters and the time window are kept the same and the five-layer parameterisation model is used. All models have misfits above one, though the minimum misfit for the second set of NA parameters (NA2: $n_{iter} = 1000$, $n_s = 150$ and $n_r = 50$) is lower than for the first set of parameters (NA1: $n_{iter} = 2000$, $n_s = 20$ and $n_r = 15$). The data thus requires a broader search than the synthetic tests. The velocity models (figure 14) are not very similar. The run with the second set of NA parameters doesn't find a sediment layer and both show a large velocity jump, but at different depths.

The observed and predicted RFs are not the same either, as visible in figure 15. The RF corrsponding to the first set of NA parameters matches the first peak of the observed RF in amplitude, timing and period, whereas the RF of the second set of NA parameters has a shorter time shift and a higher amplitude. On the other hand this RF is not as flat as the RF of the first set of NA parameters and thus matches the observations better.

Plotting of all model samples in the model space gives similar results for both runs: the occurence of several local minima for nearly all model parameters. Further, the model space is better searched for the second set of NA parameters than for the first set, as was expected.

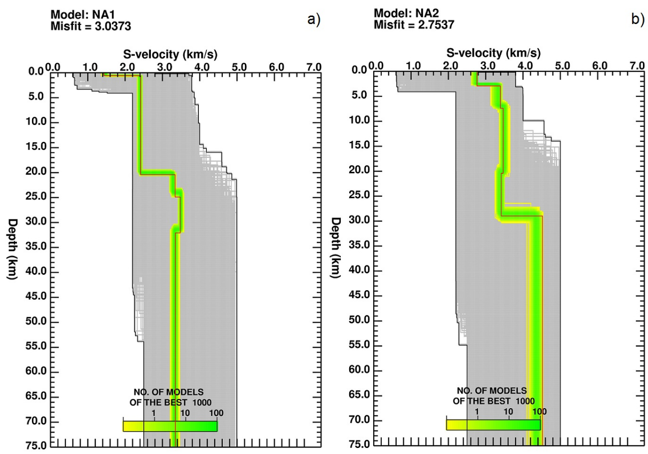

Figure 14: Velocity models for two different sets of NA parameters for station NE014. $\alpha = 2$, $c = 0.001$, $\Delta t = 25$ s. (a) NA1: $n_{iter} = 2000$, $n_s = 20$ and $n_r = 15$. (b) NA2: $n_{iter} = 1000$, $n_s = 150$ and $n_r = 50$.

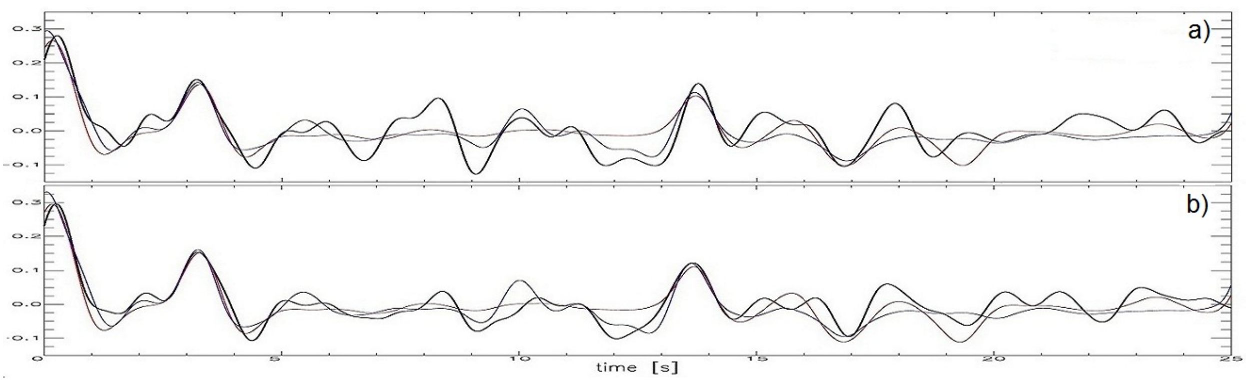

Figure 15: Observed (black) and predicted receiver functions for different NA parameters (NA1 - red, NA2 - blue) and different slownesses for station NE014. $\alpha = 2$, $c = 0.001$, $\Delta t = 25$ s. (a) $s = 0.045 - 0.050$ s/km. (b) $s = 0.050 - 0.055$ s/km.

Parameterisation model 4			
Layer	V_s [km/s]	V_p/V_s	Thickness [km]
1	0.8 - 1.6	2.40 - 3.80	1 - 3
2	2.2 - 4.0	1.50 - 2.80	1 - 30
3	2.2 - 4.4	1.20 - 2.60	1 - 30
4	2.2 - 4.4	1.20 - 2.40	1 - 30
5	2.5 - 5.4	1.20 - 2.20	5 - 50

Table 4: Five-layer starting velocity model of the NA for station NE05.

5.2 Station NE05

Since there is data available over a longer period for station NE05, for more slowness clusters a good stack could be made and the amount of RFs per stack is increased (see appendix A). The clusters that are used are $s = 0.040 - 0.045$ s/km ($\Delta = 90^{\circ}-85^{\circ}$), $s = 0.045 - 0.050$ s/km ($\Delta = 85^{\circ}-78^{\circ}$), $s = 0.050 - 0.055$ s/km ($\Delta = 78^{\circ}-70^{\circ}$) and $s = 0.065 - 0.070$ s/km ($\Delta = 55^{\circ}-45^{\circ}$), all having a NE back azimuth. Because of the larger amount of data, the prospects for station NE05 are better than for NE014. The higher range of slownesses might resolve the trade-off between the S-velocity and the thickness. Here, the more explorative set of NA parameters is used (NA2: $n_{iter} = 1000$, $n_s = 150$ and $n_r = 50$). An attempt has been made to further improve the quality of the results by first decreasing the time window, Δt, over which the misfit is calculated. This will enhance the first peaks of the RF that contain clear information on the crust-mantle transition. The time window is lowered to 15 s. This is the minimum time window, otherwise the phase reflected and converted at the Moho, PpPs, is not involved anymore. This crustal reflection is important, for it gives constraints on the thickness and velocity of the crust [33]. In the second place, the set of Gaussian parameters is changed to see if better results can be obtained by in- or decreasing the amount of detail of the RF. This will influence the ambiguity of the results as well. Again, only the results of the joint inversions are shown. Since previous studies [25, 5] found a thicker sediment layer beneath station NE05 compared to station NE014, the five-layer model is adapted. This parameterisation model can be found in tabel 4.

5.2.1 Influence of Gaussian parameters

To improve the results three sets of Gaussian parameters are tested:

1. $\alpha = 2$, $c = 0.001$ (the original set of Gaussian parameters)
2. $\alpha = 1$, $c = 0.01$
3. $\alpha = 3$, $c = 0.01$

A change in the width of the Gaussian filter will influence both the amount of detail of the RF and the ambiguity of the velocity models. The other parameters are kept constant: $n_{iter} = 1000$, $n_s = 150$, $n_r = 50$ and $\Delta t = 15s$. The five-layer model shown in table 4 is used as parameterisation model.

For all three runs the misfits for their optimum models decreased significantly compared to NE014, ranging from 0.47 to 0.67. The trend in misfit is peculiar, since the run for $\alpha = 2$ has the smallest misfit implying that the Gaussian parameters were set correctly. Probably, the RF with $\alpha = 2$ has enough detail to distinguish the most important peaks, but does not give too ambiguous results. Note that the amount of models with a misfit smaller than one is lower for the run with $\alpha = 2$ and $c = 0.001$. At first glance, the three velocity models (figure 16) look not so similar, although they have some features in common. The sediment layer is clearly resolved and has a thickness of 1-2 km with a shear wave velocity of 1.0 km/s. Further, there seems to be a velocity change at a depth of 10-15 km. The exact size of the velocity discontinuity, however, is different for the three models. The deeper structure is poorly determined, especially for $\alpha = 2$ and $\alpha = 3$, for they do not show a S-velocity comparable to typical mantle velocities of 4-5 km/s. Moreover, it can be noted that the velocity curve of $\alpha = 3$ needs more small velocity steps than the other two velocity curves to be able to produce a higher frequency RF.

In figure 17 the observed and predicted RFs are shown for the four slowness clusters. The amplitude of the RFs increases with slowness as discussed earlier. The frequency variation between the RFs with different Gaussian parameters is clearly visible. The first peak is shifted and the synthetic RFs can reproduce this time shift fairly well. The difference in amplitudes of the first peak is very small as well, although a bit higher for the RF with $\alpha = 1$. The main shape of the RFs is reconstructed, but the higher frequency variations have often slightly different timing or amplitude. This effect increases with increasing α.

When looking at the plots of all the model samples in the model space, a few trends keep appearing. All three runs show the trade-off between the thickness and the S-velocity in the first layer. Further, the second layer is poorly determined for all runs due to the small thickness of this layer. The results for $\alpha = 3$ are clearly more non-unique than for the others. Two local minima appear and the ranges of models with good fits are much wider than for the other two runs. A small second minimum appears for $\alpha = 2$ as well, so the amount of ambiguity increases with increasing α. For all three sets of Gaussian parameters the model space is searched well.

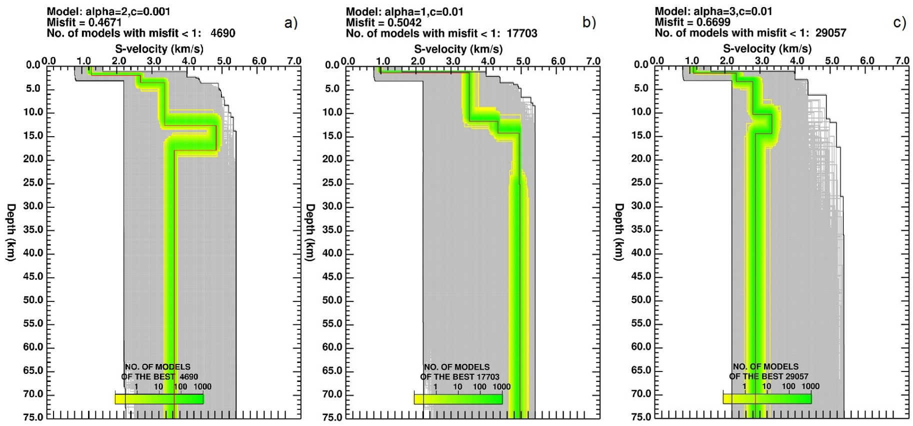

Figure 16: Velocity models for different Gaussian parameters for station NE05. (a) $\alpha = 2$, $c = 0.001$. (b) $\alpha = 1$, $c = 0.01$. (c) $\alpha = 3$, $c = 0.01$.

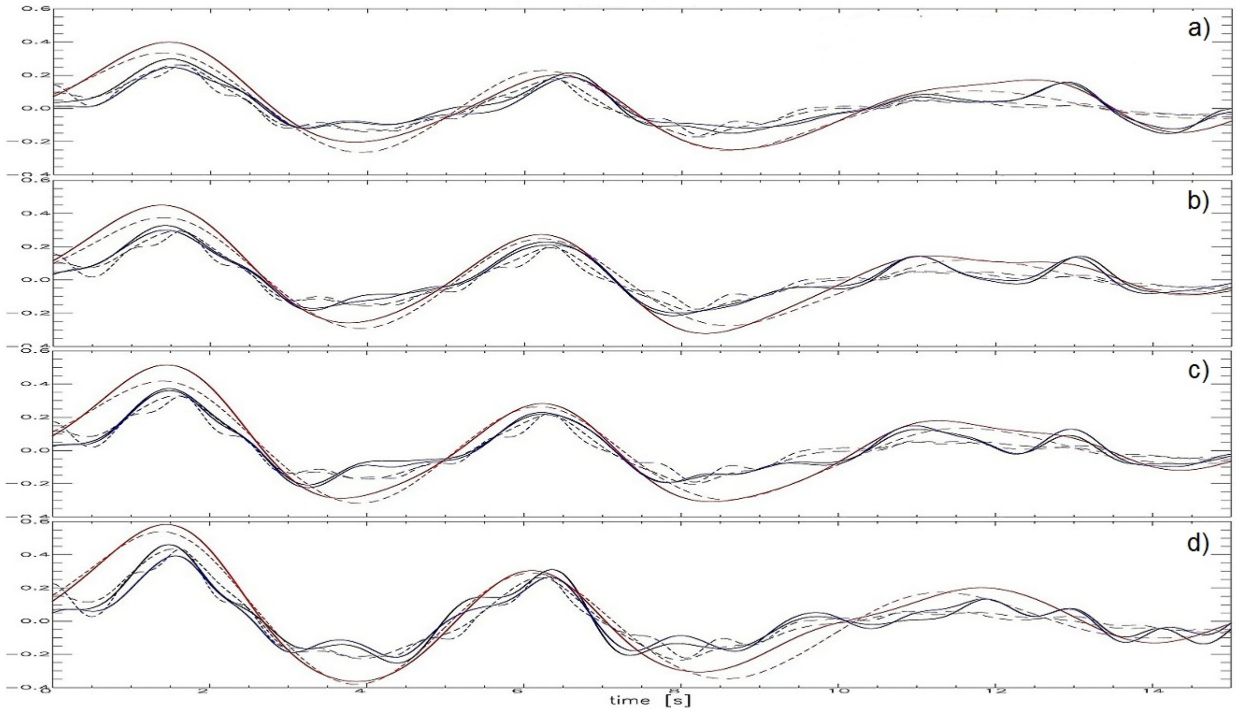

Figure 17: Observed (solid lines, black - $\alpha = 2$, $c = 0.001$, red - $\alpha = 1$, $c = 0.01$, blue - $\alpha = 3$, $c = 0.01$) and predicted (corresponding dashed lines) receiver functions for different Gaussian parameters for station NE05. (a) $s = 0.040 - 0.045 s/km$. (b) $s = 0.045 - 0.050 s/km$. (c) $s = 0.050 - 0.055 s/km$. (d) $s = 0.065 - 0.070 s/km$.

5.2.2 Influence of parameterisation models

To find the best combination of detail and uniqueness, several different parameterisation models are tested. Both the amount of layers and the ranges of the thickness, velocity and velocity ratio are changed. The results of the best four-, five- and six-layer model are presented here and the specifications can be found in table 3 (four- and six-layer models) and 4 (five-layer model). These models are tested using the second, more explorative set of NA parameters ($n_{iter} = 1000$, $n_s = 150$ and $n_r = 50$) and for both $\alpha = 1$, $c = 0.01$ and $\alpha = 2$, $c = 0.001$. Runs with both sets of Gaussian parameters are done, because for $\alpha = 2$ a better misfit of the optimum model was found, while for $\alpha = 1$ the results showed less ambiguity.

For $\alpha = 1$ and $c = 0.01$, the run with the four-layer model failed to find a model with a misfit lower than 1. Using the five- and six-layer models misfits of 0.50 and 0.60 were obtained, respectively. For $\alpha = 2$ and $c = 0.001$ all starting models provide a best model with a misfit lower than one. For both sets of Gaussian parameters the amount of models with a misfit below one increase with the number of layers. Similar features as before can be seen in the velocity models (figure 18) such as the sediment layer and the velocity contrast at $\sim$10 km depth. This velocity contrast is not obtained in the four-layer model for $\alpha = 1$. The structure at depth is again badly resolved. Furthermore, the range of well fitting models becomes wider for models with more layers. For example in the six-layer models the S-velocity of the sediments has a range of more than one km/s.

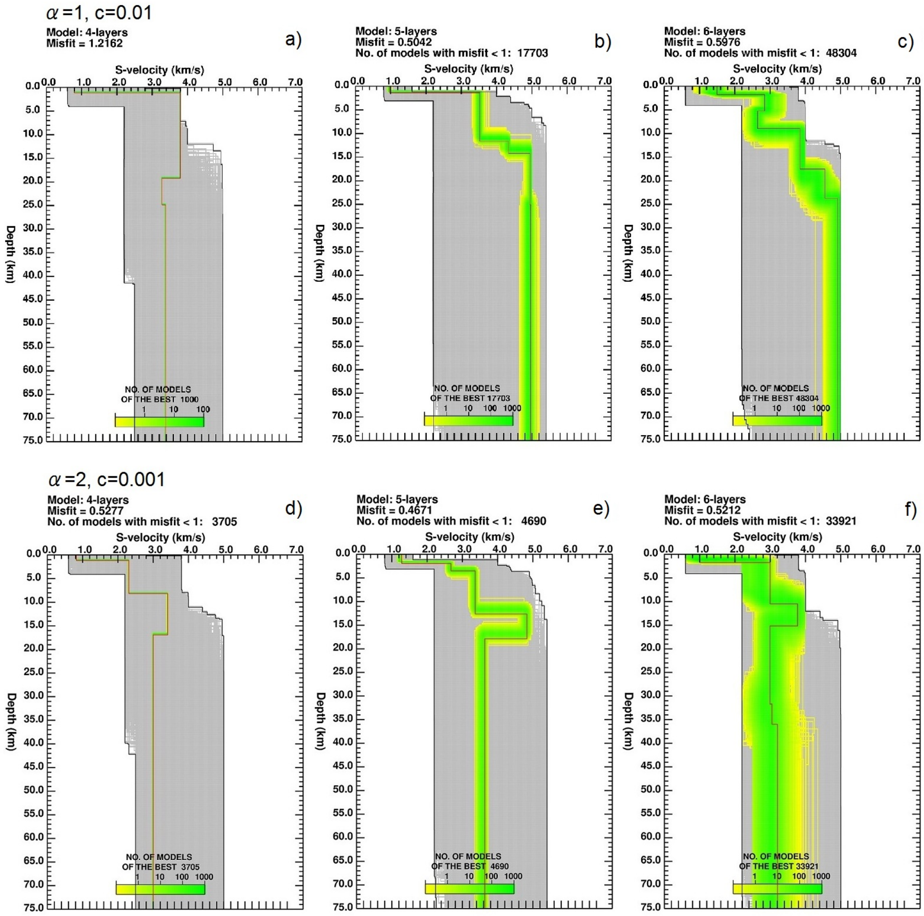

Figure 18: Velocity models for three different parameterisation models for station NE05. $n_{iter} = 1000$, $n_s = 150$, $n_r = 50$ and $\Delta t = 15s$. (a) $\alpha = 1$, $c = 0.01$, Four-layer model. (b) $\alpha = 1$, $c = 0.01$, Five-layer model. (c) $\alpha = 1$, $c = 0.01$, Six-layer model. (d) $\alpha = 2$, $c = 0.001$, Four-layer model. (e) $\alpha = 2$, $c = 0.001$, Five-layer model. (f) $\alpha = 2$, $c = 0.001$, Six-layer model.

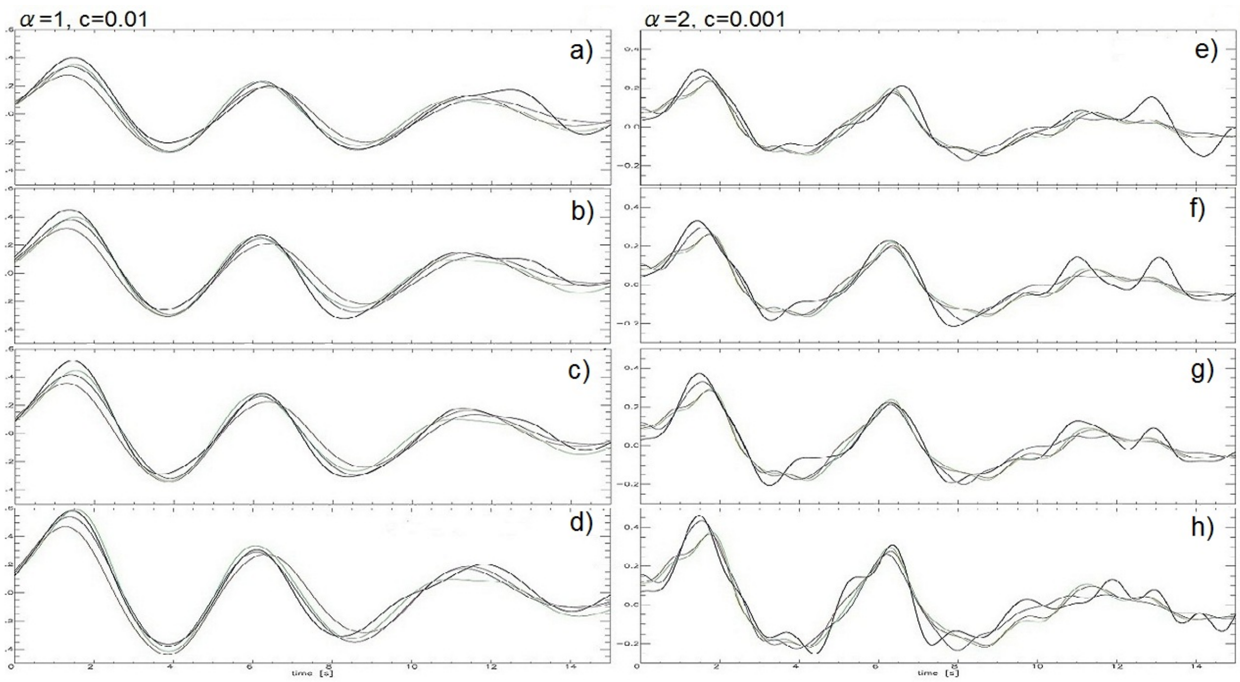

Figure 19: Observed (black) an predicted (red - model 1, green - model 4, blue - model 3) receiver functions for three different starting models and varying slowness. $n_iter = 1000$, $n_s = 150$, $n_r = 50$ and $\Delta t = 15s$. (a) $\alpha = 1$, $c = 0.01$, $s = 0.040 - 0.045$ s/km. (b) $\alpha = 1$, $c = 0.01$, $s = 0.045 - 0.050$ s/km. (c) $\alpha = 1$, $c = 0.01$, $s = 0.050 - 0.055$ s/km. (d) $\alpha = 1$, $c = 0.01$, $s = 0.065 - 0.070$ s/km. (e) $\alpha = 2$, $c = 0.001$, $s = 0.040 - 0.045$ s/km. (f) $\alpha = 2$, $c = 0.001$, $s = 0.045 - 0.050$ s/km. (g) $\alpha = 2$, $c = 0.001$, $s = 0.050 - 0.055$ s/km. (h) $\alpha = 2$, $c = 0.001$, $s = 0.065 - 0.070$ s/km.

The observed and predicted receiver functions (figure 19) are very alike, although the small bump at 14 s, most likely corresponding to the Moho reflector, PpPs [33], is not visible in any of the predicted RFs. For $\alpha = 2$ the first peak of the synthetic RFs of the four- and five-layer model has a smaller period and a slightly smaller amplitude than the observed RF.

For the five-layer parameterisation model for $\alpha = 2$ a plot of the model space with all the models analysed by the NA is given in figure 20. The trade-off between the thickness and S-velocity is clearly visible in the first layer and occurs in the other runs as well. Further, the solution is not unique due to the presence of a local minimum and the quite wide ranges of good-fitting models. These marks are present in the six-layer models as well. The amount of uniqueness increases for a decreasing amount of layers. As a last, the $v_p - v_s$ ratio is poorly resolved in most layers.

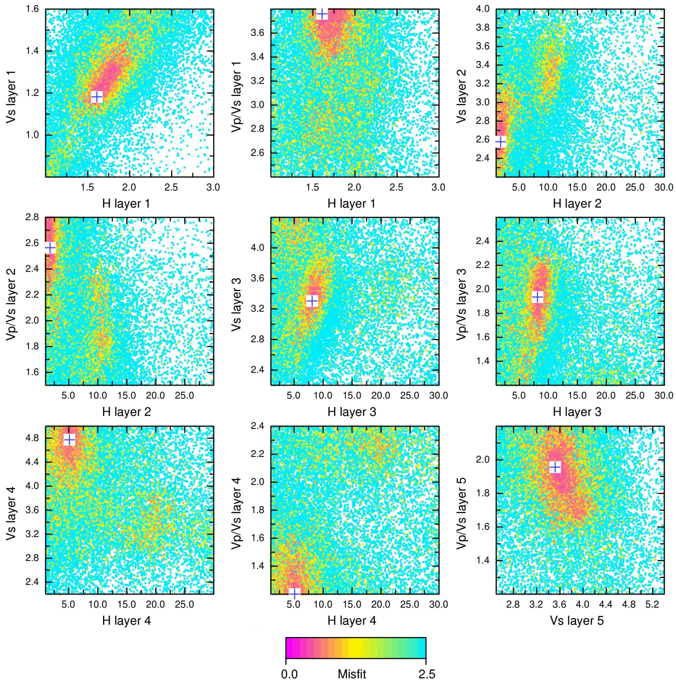

Figure 20: Plot of all model samples analysed by the NA with their misfit. On the axes the model parameters are given. Run for staion NE05 for parameterisation model 4, $\alpha = 2$, $c = 0.001$, $\Delta t = 15$ s, $n_{iter} = 1000$, $n_s = 150$ and $n_r = 50$.

6 Discussion

The determination of the crustal structure from the inversion of RFs is a good working method and the NA is able to efficiently find a good model, for the synthetic tests gave excellent results. The original and modelled RFs were very similar and the found crustal structure matched the original velocity model fairly well. The choice of the deconvolution parameters, input starting model and NA parameters have a significant influence on the search and final outcome and is highly dependent on the type of inverse problem. The data required a broader search than the synthetic tests, since no noise was added to the RFs in the synthetic tests and the real Earth structure is obviously more complex than the structures used for the synthetic tests. In finding a good set of parameters the trick is to find a good combination of detail without too much ambiguity. Both ambiguity and detail increase with the amount of layers of the parameterisation model and with α. For example, the six-layer model in combination with $\alpha = 1$ gave reasonable results, though was too ambiguous for $\alpha = 2$. The best combination for both stations is the second set of NA parameters (NA2: $n_{iter} = 1000$, $n_s = 150$ and $n_r = 50$), a five-layer input velocity model and the original set of Gaussian parameters ($\alpha = 2$ and $c = 0.001$), although $\alpha = 1$ and $c = 0.01$ gave very good results for station NE05 as well.

During stacking the high frequency variations between the RFs, which are partly due to background noise, but can result from structural features as well, are eleminiated, so that the stack has a larger period than the single RFs. Because stacks are used for the inversion, it is hard for the forward model of the NA to construct a RF with the same frequency as the original RF, if the same Gaussian parameters are used. This issue might explain the smaller period of the four- and five-layer models for station NE05 for $\alpha = 2$ and $c = 0.001$ in figure 19.

As seen from the variations between RFs with back azimuth and from the high energy level on the transverse component, the subsurface is either heterogeneous or anisotropic [8, 21, 16]. It is possible to distinguish between anisotropy and dipping layers, when there is data available over a large azimuthal range. Nagaya et al. [16] showed that for a multilayered anisotropic structure with hexagonal symmetry, anisotropy leads to several features. First of all, a relatively high energy signal on the transverse component. Secondly, change in amplitude, or even reversal, of P-S phase waveforms on both the radial and the transverse components. This variation occurs in a two-, or four-lobed pattern, dependent on the orientation of the symmetry axis. And in the third place, shear-wave splitting of the P-S converted phases. This might be hard to directly observe in the RFs, but can be used to quantify the anisotropy. Variations with back azimuth occur as well in the presence of dipping layers, though follow a less symmetric pattern [21, 15]. Unfortunately, for both station NE05 and NE014 there is not enough azimuthal variation in the data for such analyses. In addition, isotropoic dipping layers can be distinguished from anisotropic flat layers by looking at the first arrival at the transverse component. For isotropic dipping layers the timing of the first arrival on the transverse components will coincide with that on the radial component, while for anisotropic flat layers the first arrival will be later on the transverse component than on the radial component [21]. For both stations the first arrival seems to be delayed on the transverse component (see figure 5), indicating that the sedimentary layers are anisotropic rather than dipping.

The main problem with the presence of anisotropy or heterogeneity is the forward model, for it assumes isotropic, horizontal, homogeneous layers. Some attempts have been made to construct a forward model that can handle dipping layers and anisotropy [13, 7], but these have other limitations, such as a large amount of model parameters and thus an increase of non-uniqueness [8].

From the RFs of both stations it is clear that a low-velocity layer consisiting of sediments is present in the subsurface. This can be concluded from the time shift of 1-2 s. The first peak represents the P-S converted phase at the bottom of the sediment layer and dominates the direct P arrival. The time shift is smaller for NE014 indicating that the sediment layer is either less thick or has a higher S-wave velocity.

The results of station NE014 are more non-unique than those of NE05 as becomes clear from the occurence of several local minima on the plots of the model space. Moreover, there is more variation in the velocity models of station NE014. This is most likely due to the lack of data for station NE014, so the prospects for other stations of the NARS-Netherlands are not that good.

Almost all runs did show a trade-off between the thickness and the S-velocity, especially in the first layer. This is a common problem with inversion of RFs. They are more sensitive to a velocity-thickness product than to the absolute velocity and thickness values [2], for a higher velocity is required if a wave passing through a thicker layer needs to have the same travel time. RFs with different slownesses can constrain the thickness and thus the shear wave velocity of the layer, so data over a larger slowness range is needed. Furthermore, RFs show conversions of P- to S-waves, so are mostly sensitive to variations in S-velocity and only slightly to changes in P-velocities. Therefore, the $v_p - v_s$ ratio is poorly resolved in the models.

Since RFs are very sensitive to changes in shear wave velocity, phases reflected and converted at the Moho should become clear on the RFs. However, the sediment layer beneath the Netherlands is a large velocity discontinuity as well and unfortunately this dominates the RF. The signal due to the Moho P-S conversions is therefore only a very small part of the total RF preventing the Moho to be well determined in the Netherlands. It might be possible if the peaks of Moho P-S conversions could get more weight. However, RFs have been used succesfully in other locations where sediment layers are present [8, 29, 15, 30], so that leaves the question what determines if the Moho conversions are dominated by the sediment conversions. Three factors are suggested to play a role. (1) The thickness of the sedimentary layer. (2) The size of the velocity contrast between the upper crust and the sediment layer. (3) The degree of complexity of the sediments (e.g. anisotropy, dipping layers, faults).

For both stations the thickness and shear wave velocity of the sediment layer is resolved. Beneath station NE014 there is a sediment layer of ∼1 km thick with a S-wave velocity of 1.1-1.3 km/s. Below station NE05 the sediments are slightly thicker reaching to a depth of ∼2 km with a shear wave velocity of 0.9-1.2 km/s. Duin et al. [5] found a slightly thicker sediment layer beneath station NE014 of ∼1.5 km. For station NE05 both Duin et al. and van Dedem [28] found a similar thickness of 2.0-2.5 km. Another study by Paulssen et al. [18] determined a smaller thickness of 1.2 km for the sediment layer with a shear wave velocity of ∼1.6 km/s. The other studies did not determine v_s. The results agree quite well, except for the thickness found by Paulssen et al. Several studies, e.g. Duin et al. [5], showed that the sediment layer beneath the Netherlands is variable and contains some deeper basins. This variability agrees with the difference in thickness of the sediments between station NE014 and NE05.

For station NE05 there seems to be a velocity discontinuity at a depth of 10-15 km. The velocities of the layers above and below the discontinuity are not uniquely resolved, neither is the size of the velocity jump. The discontiunity is too shallow to correspond to the Moho and is probably a transition from upper to lower crust. Both the study by Paulssen et al. and by van Dedem found the same velocity discontinuity at a depth of 11 km. From their study the absolute shear wave velocities were not well determined either due to the dominance of the sediment layer over the deeper structure.

As discussed in the methods section, probability density functions can be constructed from the ensemble of the best models of the NA. This provides information on the resolution and variance of all model parameters and might thus be useful for future studies. Furthermore, it is clear that from the inversion of RFs alone the deeper structure can not be resolved. For more reliable results on the Moho depth and the crustal velocities a combination of surface wave dispersion and receiver function data can be used, since both data sets are sensitive to other parameters. RFs are mainly sensitive to velocity contrasts and a velocity-depth product, whereas surface waves are sensitive to vertical S-wave velocity averages over different depth ranges [32, 12]. Especially, the trade-off between h and v_s could be resolved in this way. Obtaining more data will help to increase the reliability of the deeper structure as well.

7 Conclusions

Inversion of receiver functions using the Neighbourhood algorithm is a good way to determine the crustal structure as has become clear from the synthetic tests. Setting the Gaussian and NA parameters correctly is important and depends on the inversion problem. Here, the width of the Gaussian, α, and the number of layers of the parameterisation model have the largest effect on the model results.

In the Netherlands the sediment P-S conversions dominate the RFs so that the deeper structure is not well defined on them. Furthermore, the high energy level on the transverse component and the variations between the RFs show that the subsurface is lateral inhomogeneous. These two factors make it hard to determine the deeper crustal structure in the Netherlands from the inversion of RFs.

Although the Moho is not determined, the sediment layer is for both station NE05 and NE014. It is slightly thicker in the center of the Netherlands than in the eastern part, which agrees with the thickness variability of the sediment layer found in other studies. Underneath station NE05, there seems to be a velocity discontinuity at a depth of 10-15 km as well, which probably corresponds to the transition from upper to lower crust.

In future studies a joint inversion of surface waves and RFs will provide more information on the deeper crustal structure beneath the Netherlands, since surface waves can give constraints on absolute S-wave velocities and RFs on velocity contrasts. Then it might also be useful to calculate probability density functions to visualize the resolution of each model parameter.

8 Acknowledgements

I would like to thank my supervisor, Hanneke Paulssen, for she was always willing to answer my questions and to make time for discussions. I want to thank Malcolm Sambridge for providing the code for the Neighbourhood Algorithm. Furthermore, Theo van Zessen helped me with computer problems when necessary. Next, I want to thank Remi for revising my thesis. And finally, my fellow students for the pleasant atmosphere in the student room.

References

[1] C. J. Ammon. The isolation of receiver effects from teleseismic P waveforms. *Bulletin of the Seismological Society of America*, 81(6):2504–2510, 1991.

[2] C. J. Ammon, G. E. Randall, and G. Zandt. On the nonuniqueness of receiver function inversions. *Journal of Geophysical Research*, 95(B10):15303–15318, 1990.

[3] T. M. Brocher. Empirical relations between elastic wavespeeds and density in the Earth's crust. *Bulletin of the Seismological Society of America*, 95(6):2081–2092, December 2005.

[4] E. Duin, R. Rijkers, and G. Remmelts. Deep seismic reflections in the Netherlands, an overview. *Geologie en Mijnbouw*, 74(3):191–197, 1995.

[5] E. J. T. Duin, J. C. Doornenbal, R. H. B. Rijkers, J. W. Verbeek, and T. E. Wong. Subsurface structure of the Netherlands results of recent onshore and offshore mapping. *Geologie en Mijnbouw*, 85(4):245–276, 2006.

[6] R.W. Eglese. Simulated annealing : A tool for operational research. *European Journal of Operational Research*, 46:271–281, 1990.

[7] A. W. Frederiksen and M. G. Bostock. Modelling teleseismic waves in dipping anisotropic structures. *Geophysical Journal International*, 141:401–412, May 2000.

[8] A. W. Frederiksen, H. Folsom, and G. Zandt. Neighbourhood inversion of teleseismic Ps conversions for anisotropy and layer dip. *Geophysical Journal International*, 155:200–212, 2003.

[9] K. Gallagher, M. Sambridge, and G. Drijkoningen. Genetic algorithms: An evolution from Monte Carlo methods for strongly non-linear geophysical optimization problems. *Geophysical Research Letters*, 18(12):2177–2180, 1991.

[10] J. Gossler, R. Kind, S. V. Sobolev, H. Kämpf, K. Wylegalla, M. Stiller, and TOR Working Group. Major crustal features between the Harz Mountains and the Baltic Shield derived from receiver functions. *Tectonophysics*, 314:321–333, 1999.

[11] N. A. Haskell. The dispersion of surface waves on multilayered media. *Bulletin of the Seismological Society of America*, pages 17–34, 1951.

[12] J. Julià, C. J. Ammon, R. B. Herrmann, and A. M. Correig. Joint inversion of receiver function and surface wave dispersion observations. *Geophysical Journal International*, 143:99–112, 2000.

[13] C. A. Langston. The effect of planar dipping structure on source and receiver responses for constant ray parameter. *Bulletin of the Seismological Society of America*, 67(4):1029–1050, 1977.

[14] C. A. Langston. Structure under Mount Rainier, Washington, inferred from teleseismic body waves. *Journal of geophysical research*, 84(B9):4749–4762, 1979.

[15] J. Li, B. Tian, W. Wang, L. Zhao, and Z. Yao. Lateral variation in the sedimentary structure of West Bohai Bay Basin inferred from P-multiple receiver functions. *Bulletin of the Seismological Society of America*, 97(4):1355–1363, August 2007.

[16] M. Nagaya, H. Oda, H. Akazawa, and M. Ishise. Receiver functions of seismic waves in layered anisotropic media: application to the estimate of seismic anisotropy. *Bulletin of the Seismological Society of America*, 98(6):2990–3006, December 2008.

[17] T. J. Owens, G. Zandt, and S. R. Taylor. Seismic evidence for an ancient rift beneath the Cumberland Plateau, Tennessee: A detailed analysis of broadband teleseismic P waveforms. *Journal of geophysical research*, 89(B9):7783–7795, 1984.

[18] H. Paulssen, J. Visser, and G. Nolet. The crustal structure from teleseismic P-wave coda-I. Method. *Geophysical Journal International*, 112:15–25, January 1993.

[19] M. Sambridge. Geophysical inversion with a neighbourhood algorithm-I. Searching a parameter space. *Geophysical Journal International*, 138:479–494, August 1999.

[20] M. Sambridge. Geophysical inversion with a neighbourhood algorithm-II . Appraising the ensemble. *Geophysical Journal International*, 138:727–746, 1999.

[21] M.K. Savage. Lower crustal anisotropy or dipping boundaries? Effects on receiver functions and a case study in New Zealand. *Journal of Geophysical Research*, 103(B7):15069 – 15087, 1998.

[22] T. Shibutani, T. Ueno, and K. Hirahara. Improvement in the extended-time multitaper receiver function estimation technique. *Bulletin of the Seismological Society of America*, 98(2):812–816, April 2008.

[23] E. Sichien, J.-P. Henriet, T. Camelbeeck, and B. De Baets. Estimating crustal thickness in Belgium and surrounding regions from Moho-reflected waves. *Tectonophysics*, 560-561:105–119, August 2012.

[24] W. T. Thomson. Transmission of elastic waves through a stratified solid medium. *Journal of Applied Physics*, 21:89–93, 1950.

[25] Netherlands Institute of Applied Geosciences TNO. *Geological atlas of the subsurface of the Netherlands - onshore*. 2004.

[26] J. Trojanowski and M. Wilde-Piórko. S-velocity structure beneath the Bohemian Massif from Monte Carlo inversion of seismic receiver function. *Acta Geophysica*, 60(1):76–91, December 2012.

[27] W. van Dalfsen, J. C. Doornenbal, S. Dortland, and J. L. Gunnink. A comprehensive seismic velocity model for the Netherlands based on lithostratigraphic layers. *Geologie en Mijnbouw*, 85(4):277–292, 2006.

[28] E. van Dedem. The crustal shear velocity structure beneath NARS-Netherlands from converted teleseismic P waves. *MSc thesis*, 1996.

[29] M. van der Meijde, S. van der Lee, and D. Giardini. Crustal structure beneath broad-band seismic stations in the Mediterranean region. *Geophysical Journal International*, 152:729–739, March 2003.

[30] L. Xu, S. Rondenay, and R. D. van der Hilst. Structure of the crust beneath the southeastern Tibetan Plateau from teleseismic receiver functions. *Physics of the Earth and Planetary Interiors*, 165:176–193, December 2007.

[31] X. Xu, X. Shen, C. Ming, G. Luo, and Y. Lin. Preliminary analysis of teleseismic receiver functions of the Ningxia and its adjacent area. *Earthquake Science*, 25:47–53, February 2012.

[32] Zhen J. Xu, Xiaodong Song, and Lupei Zhu. Crustal and uppermost mantle S velocity structure under Hi-CLIMB seismic array in central Tibetan Plateau from joint inversion of surface wave dispersion and receiver function data. *Tectonophysics*, 584:209–220, January 2013.

[33] L. Zhu and H. Kanamori. Moho depth variation in southern California from teleseismic receiver functions. *Journal of Geophysical Research*, 105(B2):2969–2980, 2000.

A Events station NE05

Date	Latitude [°]	Longitude [°]	Depth [km]	Magnitude	Slowness [s/km]	Back azimuth [°]
s = 0.040-0.045 s/km						
31/03/2002	24.28	122.18	32	7.1	0.0442	54.6
02/11/2002	2.82	96.08	30	7.4	0.0426	87.6
05/09/2004	33.07	136.62	14	7.2	0.0450	39.2
06/09/2004	33.21	137.23	10	6.6	0.0449	38.7
08/09/2004	33.14	137.20	21	6.1	0.0448	38.7
26/12/2004	3.30	95.98	30	9.1	0.0429	87.3
26/02/2005	2.91	95.59	36	6.8	0.0429	87.9
28/03/2005	2.09	97.11	30	8.6	0.0417	87.2
19/05/2005	1.99	97.04	30	6.9	0.0417	87.3
20/02/2008	2.77	95.96	26	7.4	0.0426	87.7
01/06/2008	20.12	121.35	31	6.3	0.0420	57.5
09/08/2009	33.17	137.94	292	7.1	0.0439	38.1
06/04/2010	2.38	97.05	31	7.8	0.0419	87.1
09/05/2010	3.75	96.02	38	7.2	0.0432	87.0
08/11/2011	27.32	125.62	224	6.9	0.0443	50.3
s = 0.045-0.050 s/km						
24/06/2001	44.19	148.51	33	6.0	0.0492	25.9
13/09/2002	13.04	93.07	21	6.5	0.0495	83.5
26/05/2003	38.85	141.57	68	7.0	0.0472	33.0
26/12/2004	3.30	95.98	30	9.1	0.0487	83.8
25/09/2003	41.81	143.91	27	8.3	0.0486	30.1
28/11/2004	43.01	145.12	39	7.0	0.0491	28.7
06/12/2004	42.90	145.23	35	6.8	0.0490	28.7
16/08/2005	38.28	142.04	36	7.2	0.0468	32.9
30/09/2006	46.35	153.17	11	6.6	0.0498	22.0
15/11/2006	46.59	153.27	10	8.3	0.0500	21.9
25/03/2007	37.34	136.59	8	6.7	0.0476	37.2
16/07/2007	37.53	138.45	12	6.6	0.0473	35.8
13/06/2008	39.03	140.88	7	6.9	0.0476	33.4
19/07/2008	37.55	142.21	22	7.0	0.0463	33.1
23/07/2008	39.80	141.46	108	6.8	0.0477	32.6
11/09/2008	41.89	143.75	25	6.8	0.0487	30.1
07/04/2009	46.05	151.55	31	6.9	0.0499	23.2
18/04/2009	46.01	151.43	35	6.6	0.0498	23.3
14/03/2010	37.74	141.59	32	6.5	0.0466	33.4
12/06/2010	7.88	91.94	35	7.5	0.0472	87.7
09/03/2011	38.44	142.84	32	7.3	0.0467	32.2
11/03/2011	38.30	142.37	29	9.0	0.0468	32.6
27/03/2011	38.42	142.01	19	6.2	0.0469	32.8
11/04/2011	37.00	140.40	11	6.6	0.0465	34.6
14/03/2012	40.89	144.94	12	6.9	0.0479	29.7
17/06/2012	38.92	141.83	36	6.3	0.0473	32.7
08/07/2012	45.50	151.29	20	6.0	0.0496	23.6
s = 0.050-0.055 s/km						
02/08/2001	56.26	163.79	14	6.3	0.0549	12.5
17/11/2002	47.82	146.21	459	7.3	0.0505	26.0
16/06/2003	55.49	160.00	174	6.9	0.0543	14.9
21/09/2003	19.92	95.67	10	6.6	0.0521	77.1
10/06/2004	55.68	160.00	188	6.9	0.0544	14.8
24/08/2006	51.15	157.52	43	6.5	0.0522	17.7
30/05/2007	52.14	157.29	116	6.4	0.0527	17.5
12/05/2008	31.00	103.32	19	7.9	0.0547	64.1

05/07/2008	53.88	152.89	632	7.7	0.0524	19.5
24/07/2008	50.97	157.58	27	6.2	0.0521	17.7
24/11/2008	54.20	154.32	492	7.3	0.0530	18.6
10/08/2009	14.10	92.90	24	7.5	0.0502	83.0
30/07/2010	52.50	159.84	23	6.3	0.0529	15.8
14/08/2012	49.80	145.06	583	7.7	0.0514	25.9
s = 0.065-0.070 s/km						
03/03/2002	36.43	70.44	209	6.3	0.0691	82.3
27/09/2003	50.04	87.81	16	7.3	0.0688	57.5
01/10/2003	50.21	87.72	10	6.7	0.0689	57.4
05/04/2004	36.51	71.03	187	6.6	0.0690	81.8
08/10/2005	34.54	73.59	26	7.6	0.0677	81.9
12/12/2005	36.36	71.09	224	6.5	0.0687	81.9
29/10/2009	36.39	70.72	210	6.2	0.0689	82.1
26/02/2012	51.71	95.99	12	6.7	0.0668	51.8
29/06/2012	43.43	84.70	18	6.3	0.0673	66.0

Table 5: Events recorded at station NE05 with baz = 0°-90°.

B Events station NE014

Date	Latitude [°]	Longitude [°]	Depth [km]	Magnitude	Slowness [s/km]	Back azimuth [°]
s = 0.045-0.050 s/km						
04/07/2010	39.70	142.37	27	6.3	0.0482	33.4
09/03/2011	38.44	142.84	32	7.3	0.0473	33.6
11/03/2011	38.30	142.37	29	9.0	0.0474	34.0
22/03/2011	37.24	144.00	11	6.4	0.0463	33.3
27/03/2011	38.42	142.01	19	6.2	0.0475	34.2
11/04/2011	37.00	140.40	11	6.6	0.0471	36.0
05/05/2011	38.17	144.03	11	6.0	0.0469	32.9
03/06/2011	37.28	143.91	14	6.1	0.0464	33.3
30/07/2011	36.94	140.96	30	6.3	0.0469	35.6
19/08/2011	37.67	141.65	47	6.2	0.0471	34.8
16/09/2011	40.27	142.78	35	6.7	0.0485	32.8
s = 0.050-0.055 s/km						
10/12/2009	53.42	152.76	656	6.3	0.0524	20.9
24/12/2009	42.24	134.72	392	6.3	0.0505	37.4
30/07/2010	52.50	159.84	23	6.3	0.0532	17.0
04/08/2010	51.42	-178.65	27	6.4	0.0509	3.7

Table 6: Events recorded at station NE014 with baz = 0°-90°.

C Events for Gaussian parameters

Date	Latitude	Longitude	Depth (km)	Magnitude
2009.12.10	53.42°	152.76°	656	6.3
2009.12.24	42.24°	134.72°	392	6.3
2010.02.18	42.59°	130.70°	577	6.9
2010.05.09	3.75°	96.02°	38	7.2
2010.05.24	-8.09°	-71.56°	581	6.5
2010.08.12	-1.27°	-77.31°	206	7.1
2011.01.18	28.78°	63.95°	68	7.2
2011.03.11	38.30°	142.37°	29	9.0
2011.06.22	39.96°	142.21°	33	6.7
2011.09.16	40.27°	142.78°	35	6.7

Table 7: Events used for setting the Gaussian parameters, all recorded at station NE05 and NE014.